Opposing Influence of Sensory and Motor Cortex on Striatal Circuitry and Choice Behavior

Christian R. Lee[1], Alex J. Yonk[1], Joost Wiskerke[1], Kenneth G. Paradiso[1], James M. Tepper[2], David J. Margolis[1]

[1]Department of Cell Biology and Neuroscience, Rutgers, The State University of New Jersey, New Brunswick, NJ
[2]Center for Molecular and Behavioral Neuroscience, Rutgers, The State University of New Jersey, Newark, NJ

Correspondence to:
David J. Margolis, Ph.D.
Department of Cell Biology and Neuroscience
Rutgers, The State University of New Jersey
604 Allison Road
Piscataway, New Jersey 08854 USA
+1 848 445 9533
david.margolis@rutgers.edu

Abstract

The striatum is the main input nucleus of the basal ganglia and is a key site of sensorimotor integration. While the striatum receives extensive excitatory afferents from the cerebral cortex, the influence of different cortical areas on striatal circuitry and behavior is unknown. Here we find that corticostriatal inputs from whisker-related primary somatosensory (S1) and motor (M1) cortex differentially innervate projection neurons and interneurons in the dorsal striatum, and exert opposing effects on sensory-guided behavior. Optogenetic stimulation of S1-corticostriatal afferents in *ex vivo* recordings produced larger postsynaptic potentials in striatal parvalbumin (PV)-expressing interneurons than D1- or D2-expressing spiny projection neurons (SPNs), an effect not observed for M1-corticostriatal afferents. Critically, *in vivo* optogenetic stimulation of S1-corticostriatal afferents produced task-specific behavioral inhibition, which was bidirectionally modulated by striatal PV-expressing interneurons. M1 input produced the opposite behavioral effect. Thus, our results reveal opposing roles for sensory and motor cortex in behavioral choice via distinct influences on striatal circuitry.

Introduction

The basal ganglia comprise a circuit of interconnected nuclei that are involved in a variety of behavioral functions, including sensorimotor integration and the control of voluntary movement. The striatum is the largest input nucleus of the basal ganglia, and receives afferents from numerous areas of neocortex and thalamus (Alloway et al., 2017; Assous et al., 2017); (Díaz-Hernández et al., 2018; Hooks et al., 2018; Hunnicutt et al., 2016; Klug et al., 2018; Melzer et al., 2017). In addition to promoting movement, activation of striatal neurons is also important in the termination of ongoing movement (Obeso et al., 2014; Roseberry and Kreitzer, 2017), as well as selecting an appropriate motor program and inhibiting competing motor programs (Mink, 2003). The roles of sensory and motor cortical areas in the control of movement is a fundamental unresolved issue (Ebbesen et al., 2017; Matyas et al., 2010; Sreenivasan et al., 2016). Primary sensory areas could play important roles through their corticostriatal projections, but this possibility has only recently begun to be explored (Reig and Silberberg, 2014, 2016; Sippy et al., 2015; Xiong et al., 2015).

Excitatory afferents to the striatum innervate both classes of projection neurons known as D1- and D2-receptor expressing spiny projection neurons (SPNs), as well as an increasingly appreciated diversity of interneurons, including parvalbumin (PV)-expressing, GABAergic fast spiking interneurons (Assous and Tepper, 2018; Gerfen et al., 1990, 2013; Kawaguchi, 1993; Kress et al., 2013; Muñoz-Manchado et al., 2018; Ramanathan et al., 2002; Sciamanna et al., 2015). Activation of D1-SPNs, constituting the direct pathway, tends to promote movement, while activation of D2-SPNs, constituting the indirect pathway, suppresses movement with both pathways exerting actions on other basal ganglia nuclei, and consequently on targets including the thalamus (Albin et al., 1989; DeLong, 1990; Kravitz et al., 2010; Tecuapetla et al., 2016). Conversely, striatal interneurons such as parvalbumin-expressing fast-spiking interneurons exert their effects locally by inhibiting both D1- and D2-SPNs as well as other striatal interneurons, which can have complex effects on behavior (Gittis et al., 2010, 2011; Lee et al., 2017; O'Hare et al., 2017; Tepper et al., 2010). Although most of these neuron types receive excitatory input from numerous areas of neocortex (Assous and Tepper, 2018; Hunnicutt et al., 2016), it remains unknown whether regionally distinct cortical areas differentially innervate striatal circuitry. It is possible that the balance between cortical targeting of SPNs versus interneurons is a key determinant of the behavioral effects of corticostriatal input, but this possibility has not been investigated.

Primary sensory areas of the neocortex have been extensively studied in the context of sensation and perception, but recent years have seen a greater appreciation for the role of sensory cortex in sensorimotor integration and motor control (Leinweber et al., 2017; Matyas et al., 2010; Petersen, 2014; Schneider et al., 2014). This is partly due to better understanding of the extensive interactions between sensory cortex and higher-order motor and association areas, and subcortical structures (Aronoff et al., 2010; Bosman et al., 2011; Mao et al., 2011), as well as the ability to measure and manipulate neural activity in behaving subjects (Kim et al., 2017; O'Connor et al., 2009). The primary somatosensory barrel cortex (S1) of the mouse vibrissal system is an important model system for investigating sensorimotor integration, including sensory-guided choice behavior (Diamond et al., 2008; Feldmeyer et al., 2013;

Helmchen et al., 2018). After ascending sensory input arrives from sensory thalamus at L4 barrels, layer 2/3 and L5 excitatory projection neurons route information to multiple downstream cortical and subcortical targets. S1 projections to secondary somatosensory cortex (S2) and primary motor cortex (M1) have been well studied (Chen et al., 2013a, 2015; Ferezou et al., 2007; Guo et al., 2014a; Helmchen et al., 2018; Kwon et al., 2016; Yamashita et al., 2013), but there is still little known about the circuitry or behavioral role of S1 projections to striatum. This is a major gap in knowledge because the S1-striatum projection is the largest anatomical projection from S1 (Mao et al., 2011).

We used *ex vivo* whole cell recordings of identified striatal neurons to measure the connectivity of both S1- and M1-corticostriatal inputs to striatal SPNs and PV-expressing interneurons. Further, we interrogated the roles of S1- and M1-corticostriatal inputs in regulating tactile decision making. We report substantial differences in the circuitry and behavioral effects of S1- and M1-corticostriatal inputs.

Results

Optogenetic activation of S1 or M1 corticostriatal afferents differentially engage striatal neurons

We used optogenetic activation of corticostriatal afferents from S1 or M1 with channelrhodopsin-2 (ChR2) combined with *ex vivo* whole cell current clamp recordings of identified striatal neurons to determine the striatal circuitry engaged by corticostriatal input from different sources (**Figure 1A**). Striatal D1-SPNs, D2-SPNs and PV-expressing interneurons were identified using genetically encoded fluorescent proteins and verified through their intrinsic properties in response to hyperpolarizing and depolarizing current injection (see Methods) (**Figure 1B-D**). We used current clamp recordings as opposed to voltage clamp recordings to more closely mirror the natural physiological activity of striatal neurons. Activation of ChR2-expressing S1 corticostriatal afferents with a single, brief (2.5 ms, 460 nm) light pulse induced a depolarizing postsynaptic potential (PSP) in D1-SPNs, D2-SPNs and PV-expressing interneurons (**Figure 1E-G**). PSP amplitude was larger in PV-expressing interneurons (12.81 ± 2.37 mV; n = 9 neurons) compared to D1-SPNs (2.73 ± 0.71 mV; n = 17 neurons; p = 0.000008) or D2-SPNs (3.23 ± 0.95 mV; n = 10 neurons; p = 0.0001) ($F_{(2, 33)}$ = 17.64, p = 0.000006; **Figure 1H**). Suprathreshold responses were sometimes encountered in PV-expressing interneurons, but only rarely in D1- or D2-SPNs.

We further tested the synaptic dynamics of corticostriatal inputs during train stimulation. Train stimulation (2.5 ms pulses at 25 Hz for 2 s) of S1-corticostriatal afferents to D1-SPNs (n = 5) or D2-SPNs (n = 5) led to PSPs that showed strong synaptic depression, limiting the efficacy of the input (**Figure 1I-J**). Conversely, when measured from PV-expressing interneurons (n = 4), train stimulation of S1 corticostriatal afferents led to PSPs that exhibited less depression (**Figure 1K**). Often, these PSPs exhibited slight facilitation early in the pulse train, consistent with previous findings (Sciamanna et al., 2015). When plotted as a percentage of the amplitude of the initial stimulus, the PSP evoked in PV-expressing interneurons persisted through more pulses during the stimulus train (**Figure 1L**). The largest deviations in PSP amplitudes occurred during pulses 5 to 14, and were significantly different between PV and D1-or D2-expressing

projection neurons in this stimulus range ($F_{(2, 11)}$=9.6, p=0.0039; PV vs D1 p = 0.0499; PV vs D2 p = 0.0034; D1 vs D2 p = 0.3963; **Figure 1L, M**).

In contrast to input from S1, optogenetic activation of M1 corticostriatal input evoked equally large amplitude PSPs in D1-SPNs (11.37 ± 2.25 mV; n = 13 neurons), D2-SPNs (13.35 ± 2.52 mV; n = 16 neurons) and PV-expressing interneurons (13.59 ± 3.07 mV; n = 13 neurons) ($F_{(2, 39)}$ = 0.2, p = 0.82; **Figure 2A-H**). Suprathreshold responses were routinely encountered in all neuron types in response to stimulation of M1 corticostriatal input. Train stimulation of M1 corticostriatal input to D1-SPNs (n = 5) or D2-SPNs (n = 6), as well as to PV-expressing interneurons (n = 8), led to PSPs with similarly small amounts of synaptic depression throughout the train (**Figure 2I-L**). When compared over the 5 to 14 pulse range that showed significant differences in PSP amplitudes during S1 corticostriatal stimulation, M1 corticostriatal stimulation did not lead to differences in PSP amplitude among the three neuron types ($F_{(2, 16)}$ = 0.19, p = 0.8273; **Figure 2M**). These results show that train stimulation of M1 corticostriatal afferents results in similar smaller amounts of synaptic depression in both SPNs and PV-expressing interneurons.

Together, these results indicate that S1 provides larger amplitude synaptic input to striatal PV-expressing interneurons compared to either D1- or D2-SPNs. S1 input also shows stronger short-term synaptic depression to SPNs than PV interneurons, further accentuating the biased activation of PV interneurons by S1. In contrast, M1-corticostriatal input activates D1- and D2-SPNs, and PV-expressing interneurons equally, with minimal short-term synaptic depression. Thus, the striking difference in S1- versus M1-corticostriatal innervation lies in the more efficacious innervation by S1 of PV-expressing interneurons compared to D1- and D2-SPNs.

Input-specific effects on behavioral performance

To determine the effect of S1- or M1-corticostriatal input on sensorimotor behavior, we assessed how optogenetic stimulation of these regionally specific corticostriatal inputs affected performance of a whisker-dependent texture discrimination task in head-fixed mice (**Figure 3A-C**)(Chen et al., 2013a, 2015; Lee and Margolis, 2016). In this Go/NoGo task, mice receive water reward for correct licking in response to the rough texture (Hit trial) and no water reward for licking in response to the smooth texture (False Alarm trial). Textures are presented to the whiskers via a motorized stage. An optical fiber was implanted above dorsal striatum in mice expressing ChR2 in either S1 or M1 (**Supplemental Figure 1**). We measured the effects of optogenetic stimulation on changes in Hit Rate, False Alarm Rate, Sensitivity, and Bias compared to the start of the session. Mice completed 50 trials without optogenetic stimulation followed by 77 trials with stimulation. Optogenetic stimulation of S1-corticostriatal input led to reduction in behavioral responding, as evident in a raster plot of licking in a representative session before and during stimulation (**Figure 3D**). As a result of S1-corticostriatal stimulation, we found significant reductions in Hit Rate (0.62 ± 0.08 to 0.39 ± 0.11; p = 0.005; n = 6), FA Rate (0.39 ± 0.10 to 0.21 ± 0.06; p = 0.013; n = 6), and Bias (-0.04 ± 0.31 to -0.78 ± 0.35; p = 0.011; n = 6), while Sensitivity decreased, but not significantly (0.93 ± 0.34 to 0.62 ± 0.40; p = 0.245; n = 6) (**Figure 3E**).

The behavioral effects of optogenetic stimulation of M1-corticostriatal input were markedly different, leading instead to increased behavioral responding, as seen in the raster plot of licking in a representative behavioral session (**Figure 3F**). M1-corticostriatal stimulation led to a significant increase in FA Rate (0.33 ± 0.04 to 0.63 ± 0.10; p = 0.013; n = 6; **Figure 3G**) reflecting an overall increase in responding. Hit Rate (0.72 ± 0.06 to 0.82 ± 0.05; p = 0.285; n = 6), Sensitivity (1.53 ± 0.28 to 0.80 ± 0.32; p = 0.086; n = 6), and Bias (0.24 ± 0.17 to 0.90 ± 0.26; p = 0.071; n = 6) did not change significantly (**Figure 3G**).

The effects of both S1- and M1-corticostriatal stimulation were specific to the texture discrimination task, as we observed no overall effect on open field or rotarod performance (**Supplemental Figure 2**). Furthermore, trimming the whiskers significantly impaired behavioral performance on the texture discrimination task, demonstrating that the task is dependent on whisker-based tactile input (**Supplemental Figure 3**).

Overall, the results of decreased behavioral responding during S1-corticostriatal stimulation and increased behavioral responding during M1-corticostriatal stimulation indicate opposing effects of S1 and M1 inputs to striatum on sensory-guided behavior.

Optogenetic stimulation of striatal PV interneurons suppresses responding in the tactile discrimination task

How do S1- and M1-corticostriatal inputs lead to opposite effects on behavior? We hypothesized that the biased activation of PV-expressing interneurons by S1 could play a key role. Therefore, we tested whether direct optogenetic activation of PV- expressing interneurons caused a similar behavioral effect as S1 optical stimulation (**Figure 4A-C**). An optical fiber was implanted above dorsal striatum in mice expressing ChR2 in PV-expressing interneurons, and mice were trained on the task as above. Mice completed 50 trials without optogenetic stimulation followed by 77 trials with direct stimulation of PV-expressing interneurons. Optogenetic stimulation of striatal PV interneurons led to a reduction of behavioral responding, as shown in a representative session (**Figure 4D**). Overall, Hit Rate (0.60 ± 0.08 to 0.42 ± 0.12; p = 0.007; n = 6), FA Rate (0.29 ± 0.03 to 0.19 ± 0.04; p = 0.01; n = 6), and Bias (-0.18 ± 0.18 to -0.72 ± 0.34; p = 0.03; n = 6; **Figure 4E**) decreased significantly, while Sensitivity (1.00 ± 0.37 to 0.57 ± 0.50; p = 0.053; n = 6; **Figure 4E**) also decreased, but not significantly. Thus, direct stimulation of PV-expressing interneurons exerts a suppressive influence on behavioral responding, similar to S1-corticostriatal stimulation.

PV cell suppression abolishes inhibitory effects of S1 stimulation on behavior

Our results thus far suggested that striatal PV interneurons mediate the suppressive effects of S1 on behavior. We next tested whether inhibiting these interneurons could attenuate or reverse the behavioral inhibition produced by S1 stimulation. We tested this in mice expressing halorhodopsin (NpHR) in striatal PV-expressing interneurons and ChR2 in S1 corticostriatal afferents. Mice were again trained on the texture discrimination task. Mice performed 40 baseline trials, followed by 40 S1-ChR2 optical stimulation trials, followed by 47 trials with S1-ChR2 stimulation and concurrent inhibition of PV-expressing interneurons with NpHR (460 plus 520 nm). We found that optogenetic inhibition of PV-expressing interneurons could reverse the suppressive effect of S1-corticostriatal stimulation on behavior as shown in a representative

session (**Figure 4F**) and reflected in significant differences for all behavioral parameters among the three conditions (repeated measures ANOVA: Hit Rate ($F_{(2, 6)}$ = 9.66, p = 0.0133; n = 4), FA Rate ($F_{(2, 6)}$= 7.08, p = 0.0264; n = 4), Sensitivity ($F_{(2, 6)}$ = 8.18, p = 0.0193; n = 4), and Bias ($F_{(2, 6)}$ = 10.6, p = 0.0107; n = 4) (**Figure 4G**). Paired contrasts revealed a significant decrease in Hit Rate following optogenetic stimulation of S1 corticostriatal afferents, as expected (p = 0.0426). Strikingly, Hit Rate increased significantly following simultaneous stimulation of S1 corticostriatal afferents and optogenetic inhibition of PV-expressing interneurons (p = 0.0088) returning to control levels (baseline vs. dual stim; p = 0.8353). Similarly, there was a significant decrease in FA Rate following S1 corticostriatal stimulation (p = 0.0078) which was lost with simultaneous inhibition of PV-expressing interneurons (baseline vs. dual stim; p = 0.3105). Changes in Sensitivity and Bias induced by S1 corticostriatal stimulation were also reversed by simultaneous inhibition of PV-expressing interneurons (**Figure 4G**). Sensitivity increased significantly following simultaneous S1 corticostriatal stimulation and inhibition of PV-expressing interneurons compared to stimulation of S1 input alone (p = 0.0375; baseline vs. dual opto; p = 0.0559). Bias decreased significantly following S1 corticostriatal stimulation (p = 0.0095) as expected, and returned to control levels during simultaneous inhibition of PV-expressing interneurons (S1 stim vs dual opto p = 0.0361; baseline vs. dual opto; p = 0.6936).

Thus, our results indicate that S1-corticostriatal input exerts an inhibitory influence on sensory-guided behavior, opposite the effects of M1-corticostriatal input. The behavioral inhibition could be reproduced by direct striatal PV interneuron activation, and furthermore could be restored by suppression of PV interneurons during S1-corticostriatal activation. Our results highlight a novel role for S1 in corticostriatal circuitry and behavior, and implicate striatal PV interneurons as key players in this process.

Discussion

Here we have shown that corticostriatal inputs from sensory and motor cortical areas differentially engage neurons in the striatum, leading to distinct influences on behavior. Specifically, S1-corticostriatal input primarily activates PV-expressing interneurons and suppresses responding in a tactile discrimination task, while M1-corticostriatal input activates SPNs and PV-expressing interneurons equally and produces increased responding in the task. Bidirectional optogenetic manipulations also revealed a central role for striatal PV-expressing interneurons in behavioral control. These are the first data to show that differential activation of striatal neurons by discrete neocortical areas leads to opposite effects on sensory-driven behavior.

The role of the basal ganglia in response inhibition

For nearly three decades, it has been appreciated that the basal ganglia are involved in both the promotion of movement through activation of direct pathway SPNs and the suppression of movement through activation of indirect pathway SPNs (Albin et al., 1989; DeLong, 1990). Natural movements are complex and require the activation of some motor programs and the suppression of others resulting in the activation of both pathways during behavior (Mink, 1996, 2003; Tecuapetla et al., 2016). However, the movement promoting influence of the direct

pathway and the movement suppressing influence of the indirect pathway is supported by the bulk of available evidence (Kravitz et al., 2010; Tecuapetla et al., 2016). The mechanisms which could lead to activation of one striatal pathway over the other have remained incompletely understood, though the demonstrated role of the hyperdirect pathway from cortex to the subthalamic nucleus of the indirect pathway in stopping ongoing movements has strengthened the idea that differential activation of the direct and indirect pathways can bias behavior (Jahfari et al., 2011; Schmidt et al., 2013). Here we demonstrate an additional pathway for action suppression through S1 corticostriatal input preferentially activating PV-expressing interneurons. An earlier study using electrical stimulation of primate sensory cortex and immediate early gene expression in striatum also suggested a preferential activation of striatal PV-expressing interneurons by S1 activation (Parthasarathy and Graybiel, 1997). It appears increasingly plausible that S1 is an important mediator of behavioral control through its actions on striatal PV interneurons.

Striatal PV-expressing interneurons are recruited to inhibit action

Striatal PV-expressing interneurons are powerfully activated by cortical inputs and inhibit SPNs (Bennett and Bolam, 1994; Koós and Tepper, 1999; Mallet et al., 2005). Behaviorally, inhibiting PV-expressing interneurons can cause dyskinesias, and these neurons are decreased in a mutant mouse which also exhibits hyperkinetic behaviors (Burguière et al., 2013; Gittis et al., 2011). A previous study also showed that optogenetic activation of PV-expressing interneurons tended to decrease responding in a behavioral task (Tecuapetla et al., 2016). Overall, it would appear that PV-expressing interneurons act to suppress movement. This is consistent with our results which indicate that S1 corticostriatal inputs preferentially activate striatal PV-expressing interneurons and suppress responding in the tactile discrimination task. One mechanism that might underlie this effect is the slight preference for PV-expressing interneurons to innervate direct pathway SPNs (Gittis et al., 2010). Our data showing stronger short term synaptic depression in S1 inputs to SPNs compared to PV interneurons could accentuate the bias toward PV interneuron activation. It is plausible that corticostriatal input from S1 would lead to preferential inhibition of D1-expressing striatonigral SPNs, thus disinhibiting the inhibitory output of the basal ganglia from the substantia nigra pars reticulata/internal globus pallidus/entopeduncular nucleus and suppressing movement.

Roles for sensory and motor cortex striatal signaling

S1 barrel cortex has long been recognized as a key locus for whisker-guided behaviors. While S1 is densely interconnected with many cortical and subcortical areas, including thalamus, higher-order sensory cortex, motor cortex, and association cortex, among many others (Aronoff et al., 2010; Bosman et al., 2011; Mao et al., 2011), the detailed circuitry and behavioral roles of these pathways are just beginning to be understood (Crochet et al., 2018; Ni and Chen, 2017). For example, S1 interactions with M1 and S2 have been found to be important for detection of sensory stimuli, behavioral performance, and learning (Chen et al., 2013a, 2015; Ferezou et al., 2007; Guo et al., 2014a; Kwon et al., 2016; Xu et al., 2012; Yamashita and Petersen, 2016). One of the largest anatomical projections from both S1 and M1 (larger than to M1 and S2) is to the dorsolateral striatum (Guo et al., 2015; Mao et al., 2011). *In vivo* recordings have found that

both D1 and D2 SPNs receive whisker-driven synaptic input (Reig and Silberberg, 2014; Sippy et al., 2015), but differences between S1 and M1 input, and potential recruitment of identified interneurons was not investigated. Remarkably, in spite of the potential importance of corticostriatal signaling for sensorimotor function, the circuitry and behavioral impact of S1- and M1- corticostriatal projections remained unresolved.

Our results show that S1 input more strongly innervates striatal PV-expressing interneurons than M1 input. This difference in circuitry has profound effects on behavior, with S1-corticostriatal activation leading to behavioral inhibition instead of activation. These results represent a previously unappreciated role for S1-corticostriatal inputs and have major implications for understanding how the striatum integrates inputs from different cortical and subcortical sources to produce behavioral responses. In future studies it will be important to identify which corticostriatal cell types mediate S1 signaling, the dynamics of S1 and M1 activity during behavior, and whether other interneuron cell types are innervated by S1 and M1 inputs, among many other fascinating avenues opened up by our study.

Conclusions

We have shown that input from primary sensory cortex (S1) preferentially engages striatal PV-expressing interneurons in the striatum and suppresses responding in a tactile discrimination task. Conversely, corticostriatal input from primary motor cortex (M1) engages D1- and D2-expressing SPNs as well as PV-expressing interneurons, and promotes responding in the task. Our findings suggest that corticostriatal input from regionally and functionally specific areas of cortex can have different physiological and behavioral consequences.

Author Contributions

CRL, AJY, JW, KGP, JMT, and DJM designed research. CRL, AJY, and JW performed research. CRL, AJY, JW, and DJM analyzed data. CRL, AJY, and DJM wrote the manuscript. All authors approved the final version of the manuscript.

Acknowledgements

The authors thank Battulga Amarbat and Neeha Pathan for assistance with running behavioral experiments, Ben Pasternak and Wahhaj Khokar for assistance with analyzing lick data and Dr. Mark West for providing D1- and D2-cre breeders. This work was supported by grants from the Rutgers Brain Health Institute Pilot Grant Program to both DJM and JMT and the National Institutes of Health (R01NS094450 and R01NS034865) to DJM and JMT, respectively.

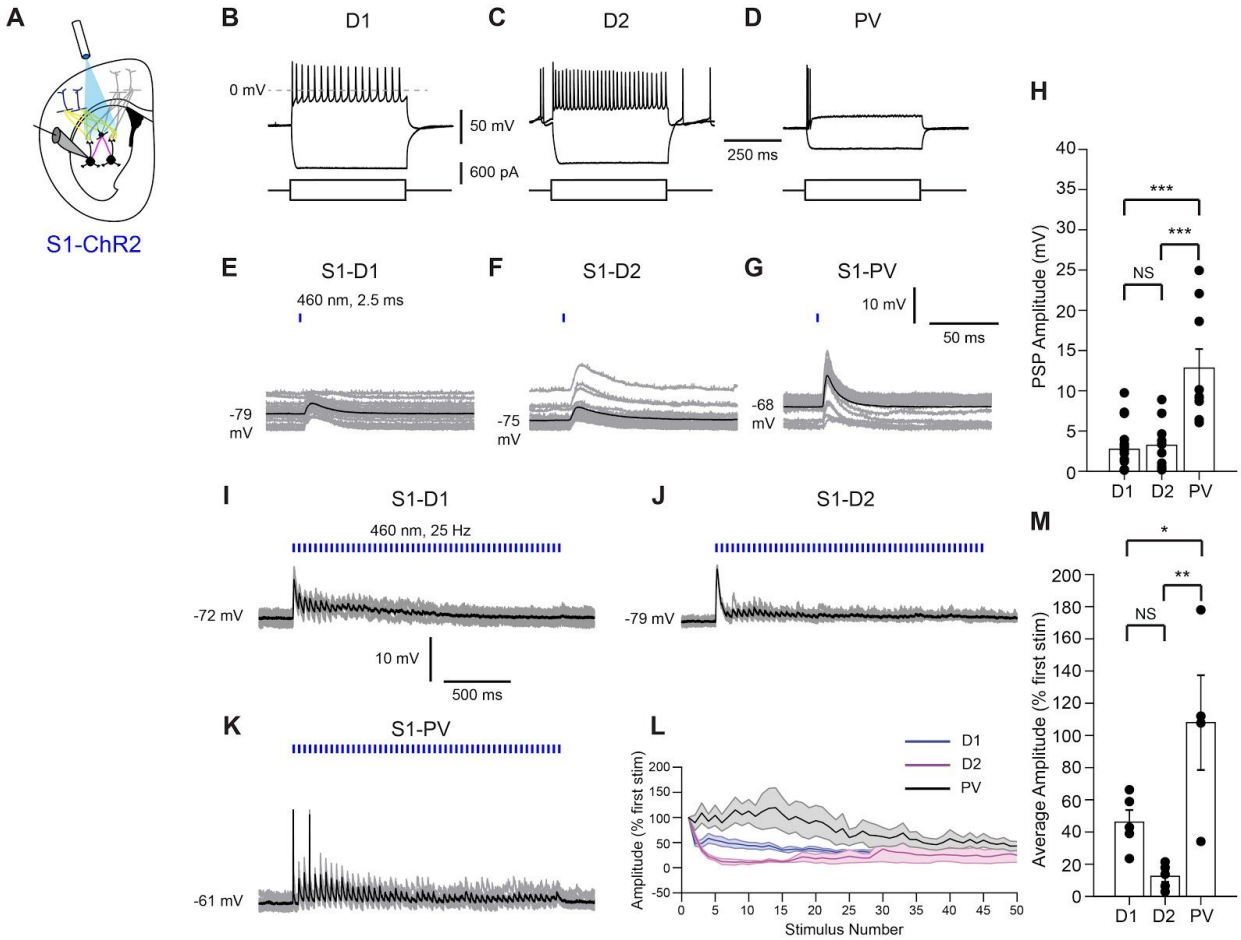

Figure 1: S1 corticostriatal input preferentially excites striatal PV-expressing interneurons. **(A)** Schematic diagram illustrating recording of striatal neurons and optogenetic activation of S1 corticostriatal afferents in an ex vivo slice. **(B)** Characteristic physiological properties of D1- and **(C)** D2-SPNs and **(D)** PV-expressing interneurons in response to hyperpolarizing and depolarizing current injection. **(E)** Postsynaptic potentials (PSPs) evoked by optogenetic stimulation of S1 corticostriatal afferents in a D1-receptor expressing SPN. The average PSP is shown in black and individual traces in gray. Optogenetic stimulation is schematized by the blue line. **(F)** The postsynaptic potential evoked in a D2-receptor expressing SPN and **(G)** a PV-expressing interneuron. **(H)** The amplitude of the PSP evoked by optogenetic stimulation of S1 corticostriatal inputs was significantly larger in PV-expressing interneurons than in D1- or D2-SPNs. **(I)** Representative responses of a D1-receptor expressing SPN to optogenetic train stimulation of S1 corticostriatal inputs. Train stimulation is schematized by the blue lines. **(J)** The same is shown for a D2-receptor expressing SPN. Both D1- and D2-receptor expressing SPNs show strong short term depression to train stimuli. **(K)** Representative response of a PV-expressing interneuron to S1 corticostriatal train stimulation. In contrast to the SPNs, train stimulation shows less synaptic depression through the train, and even some facilitation early on. Individual traces are shown in grey and the average in black. **(L)** Summary plots of the PSP amplitude for each neuron type compared to first pulse amplitude. Mean is shown with SEM shaded. Both D1 and D2-receptor expressing SPNs show stronger synaptic depression during the train while the PV-expressing interneurons show a slight initial facilitation followed by depression later in the train. **(M)** Relative PSP amplitude (mean of pulses 5 to 14 compared to first pulse) is significantly greater in PV-expressing interneurons than in D1 or D2-receptor expressing SPNs. Data shown as mean ± SEM. ***$p < 0.001$, **$p < 0.01$, *$p < 0.05$, NS = not significant.

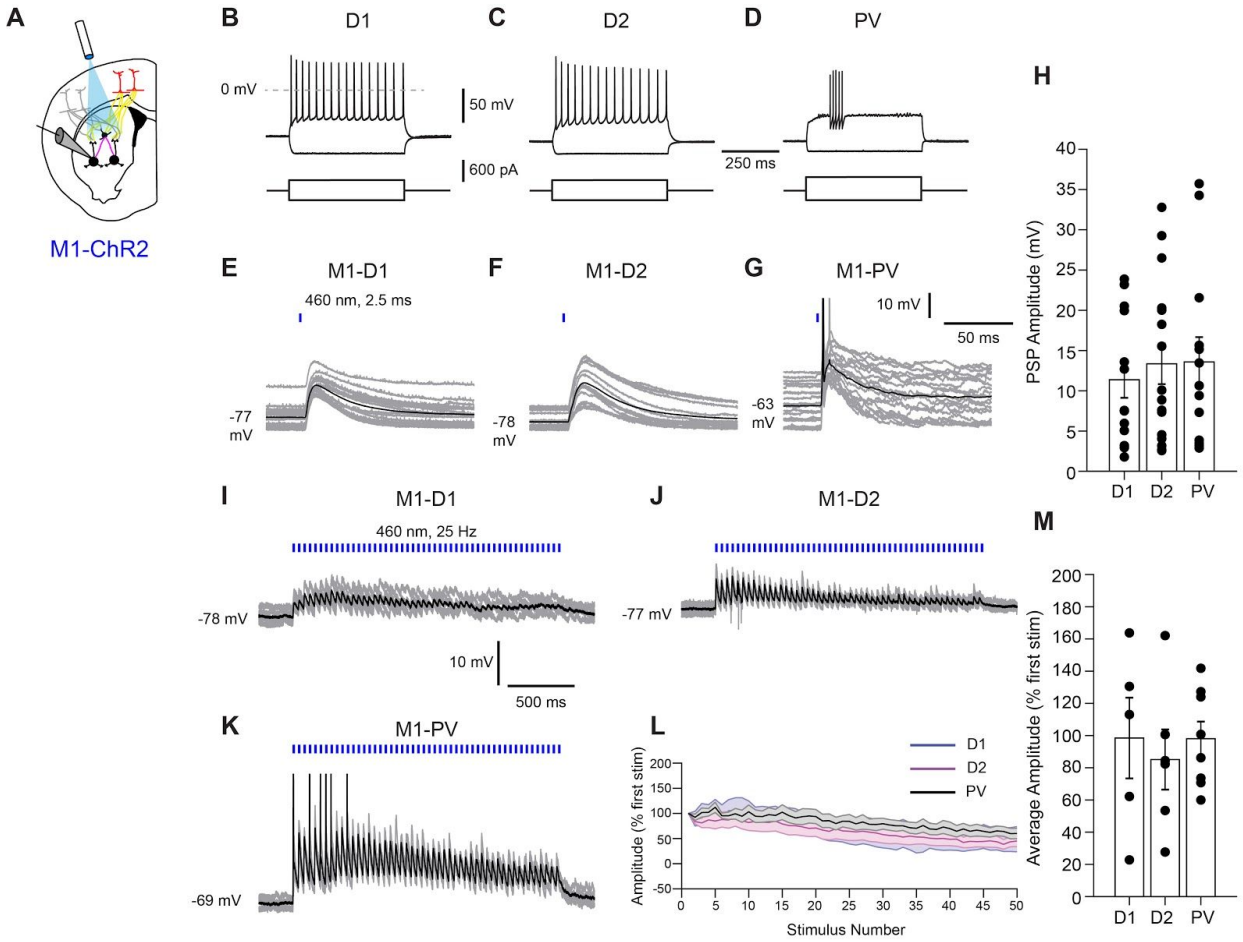

Figure 2: M1 corticostriatal input excites SPNs and PV-expressing interneurons equally. **(A)** Schematic diagram illustrating recording of striatal neurons and optogenetic activation of M1 corticostriatal afferents in an ex vivo slice. **(B)** Representative responses to hyperpolarizing and depolarizing current injection in D1-SPNs or **(C)** D2-SPNs as well as a **(D)** PV-expressing interneuron. **(E)** Postsynaptic potentials evoked by optogenetic stimulation of M1 corticostriatal afferents in a D1-receptor expressing SPN, **(F)** D2-receptor expressing SPN and **(G)** a PV-expressing interneuron. Average response shown in black and individual responses in grey. In some cases, action potentials have been truncated. Optogenetic stimulation is schematized by the blue line. **(H)** Amplitudes of PSPs evoked in each of these neuron types were similar. **(I)** Responses of a D1-receptor expressing SPN to train optogenetic stimulation of M1 corticostriatal afferents. **(J)** The same is shown for a D2-receptor expressing SPN and **(K)** a PV-expressing interneuron. Train stimulation is schematized by the blue lines. **(L)** Stimulation of these afferents induced PSPs with similar levels of synaptic depression through the train. Data plotted as mean with shaded SEM. **(M)** When compared over the same range of stimulus pulses (5 to 14) that showed large deviations in PSP amplitude during stimulation of S1 corticostriatal input, PSPs evoked by M1 corticostriatal input did not differ in amplitude. Data presented as mean ± SEM.

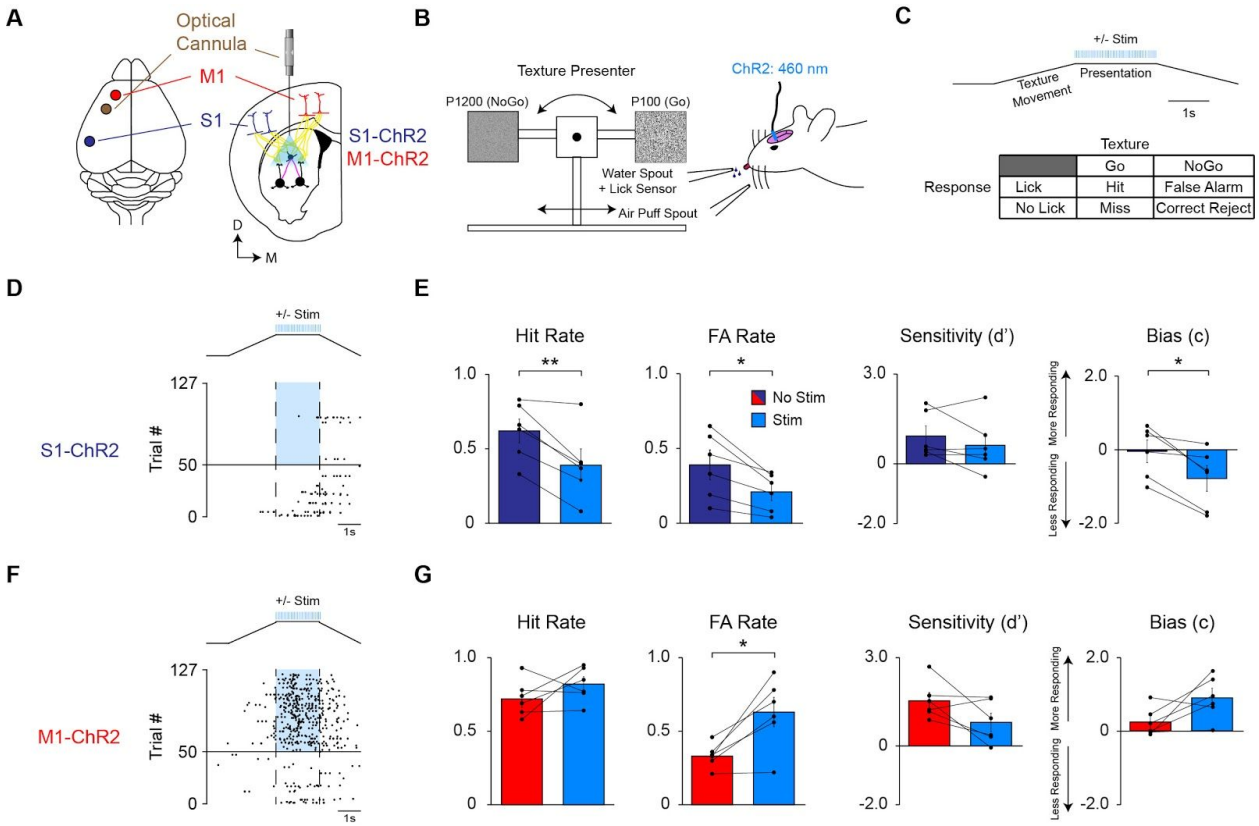

Figure 3: S1 corticostriatal input inhibits responding while M1 corticostriatal input promotes responding in a tactile discrimination task. **(A)** *Left*: Schematic dorsal view of AAV injection sites and optical cannula placement. *Right:* Schematic illustrating *in vivo* optogenetic stimulation of S1 or M1 corticostriatal afferents during a Go/NoGo task. **(B)** Schematic of optogenetic stimulation during tactile discrimination task. **(C)** *Top:* Representation of trial structure and stimulation timing. *Bottom:* Possible outcomes for each stimulus-response pair. **(D)** Raster plot showing lick responses in a single representative session before and after S1 corticostriatal stimulation. Horizontal black line indicates onset of optical stimulation at trial 50. Vertical dashed lines indicates start and end of presentation time. Blue portion between dashed lines indicates timing of optical stimulation. Timing of the trial and train stimulation is schematized above. **(E)** Effects of S1 corticostriatal stimulation (n = 6 mice) on Hit Rate, FA Rate, Sensitivity and Bias. Data are mean (± SEM) for baseline and stimulated conditions. **(F)** Raster plot showing lick responses from a representative session before and after stimulation of M1 corticostriatal afferents. **(G)** Effects of M1 corticostriatal stimulation (n = 6 mice) on Hit Rate, FA Rate, Sensitivity, and Bias. Data are mean ± SEM. Hit Rate is the proportion of successful Go trials divided by the total number of Go trials. FA Rate is the proportion of unsuccessful NoGo trials divided by the total number of NoGo trials. Sensitivity is the capacity to discriminate between the Go and NoGo texture. Bias is the overall responding during the session. *$p < 0.05$, **$p < 0.01$.

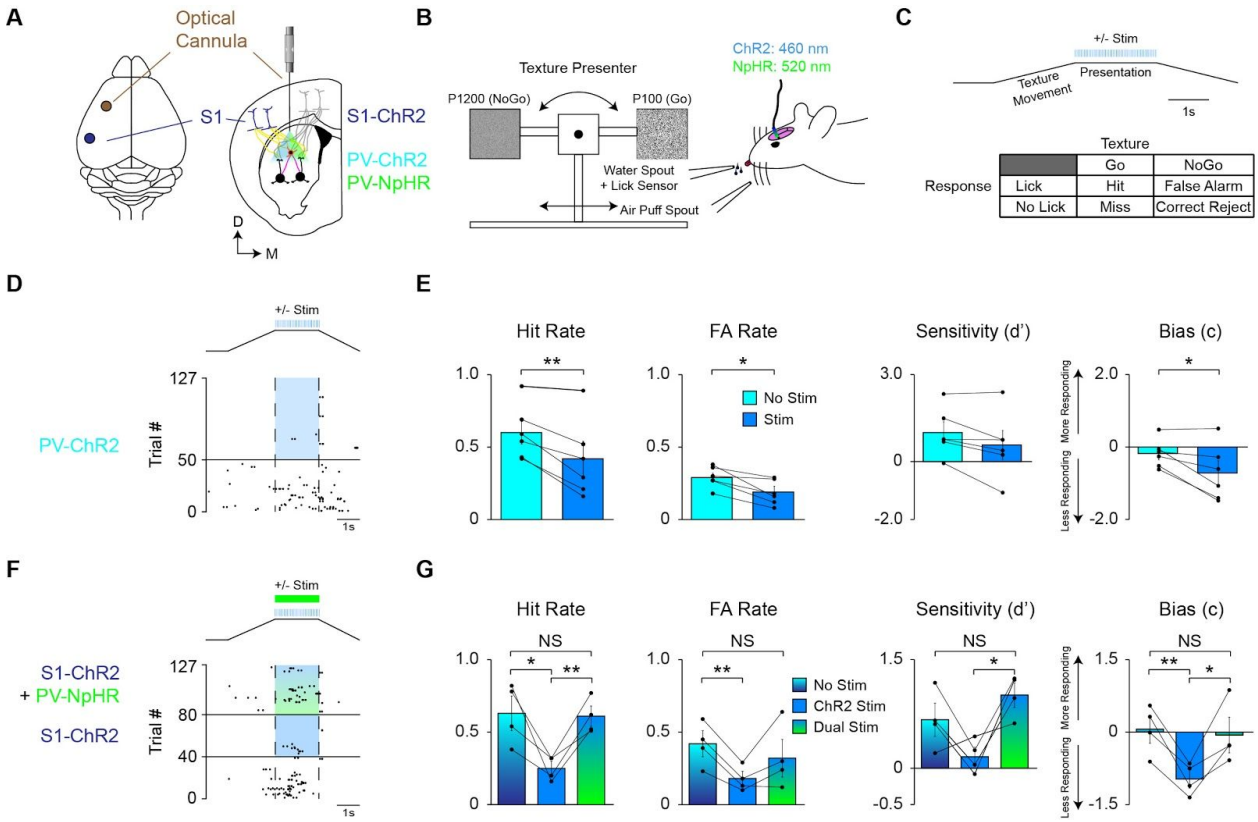

Figure 4: Response inhibition caused by S1 corticostriatal input is mediated by striatal PV-expressing interneurons. **(A)** *Left:* Schematic illustrating S1 AAV injection site and optical cannula placement. *Right:* Schematic depicting *in vivo* optogenetic stimulation of S1 corticostriatal afferents or PV-expressing interneurons as carried out during the behavioral task. **(B)** Schematic of optogenetic stimulation during tactile discrimination task. PV-expressing interneurons, also expressing ChR2 were directly stimulated with blue light (460 nm) in some experiments. In other experiments, PV interneurons were inhibited by activating NpHR with green light (520 nm), while S1 terminals were stimulated with blue light (460 nm). **(C)** *Top:* Representation of trial structure and train stimulation timing. *Bottom:* Possible outcomes for each stimulus-response pair. **(D)** Raster plot of lick responses during a representative behavioral session before and after direct activation of PV-expressing interneurons. Horizontal line indicates onset of stimulation at trial 50. The trial structure and stimulation period is schematized above and bounded by broken lines. Representative trial structure and stimulation timing. **(F)** Raster plot of lick responses during a representative behavioral session before and after optogenetic activation of S1 corticostriatal afferents as well as with simultaneous optogenetic suppression of PV-expressing interneurons with NpHR. Horizontal line at trial 40 indicates onset of S1 corticostriatal stimulation. Horizontal line at 81 indicates onset of simultaneous optogenetic suppression of PV-expressing interneurons with NpHr, as indicated by the blue/green gradient fill. Vertical dashed lines indicate start and end of presentation time. Trial structure and train stimulation of ChR2 as well as tonic activation of NpHR during the response window is schematized above. **(G)** Hit Rate, FA Rate, Sensitivity, and Bias for baseline, stimulation of S1 corticostriatal input, and simultaneous stimulation of S1 corticostriatal input and NpHR suppression of PV-expressing interneurons (n = 4 mice). Data are mean ± SEM. * $p < 0.05$, ** $p < 0.01$.

Experimental Model and Subject Details

Animals

All procedures were approved by the Rutgers University Institutional Animal Care and Use Committee (IACUC; protocol #: 13-033). All mice used in experiments were housed in a reverse light cycle room (lights off from 08:00 to 20:00) with food and water available *ad libitum*, unless subjected to water restriction during behavioral training. **Table 1** summarizes the strains of transgenic mice used. Both male and female mice were used for electrophysiological and behavioral experiments and were adult at the time of the first surgical procedures (average 7.1 weeks, range 4.1 to 13.4 weeks). During behavioral testing, daily water intake was restricted to ~1.5 mL per mouse per day. This was done to motivate performance of the behavioral task described below. Baseline body weight was measured once prior to water restriction and daily thereafter. Body weight decreased on average to 84.24 ± 0.81% of their original weight, consistent with levels of restriction used to motivate behavior (Guo et al., 2014b). All handling and behavioral experiments were conducted during the dark phase of the cycle.

Strain	Repository Number	Repository	Reference
B6.Cg-Tg(Drd1a-tdTomato)6Calak/J	016204	Jackson	(Ade et al., 2011)
B6.FVB(Cg)-Tg(DrD1cre)EY262Gsat/Mmucd	030989-UCD	Gensat	(Gerfen et al., 2013)
B6.FVB(Cg)-Tg(DrD2cre)ER44Gsat/Mmucd	032108-UCD	Gensat	(Gerfen et al., 2013)
B6.129P2-Pvalbtm1(cre)Arbr/J	008069	Jackson	(Hippenmeyer et al., 2005)
Ai14 (cre-tdTomato)	007914	Jackson	(Madisen et al., 2010)
Ai32 (cre-ChR2)	012569	Jackson	(Madisen et al., 2012)

Table 1: Summary of transgenic mice used.

Viral Vector Expression and Injection Surgery in mice

Unilateral injections of AAV1-CaMKIIa-hChR2(H134R)-eYFP.WPRE.hGH (Penn Vector Core; Addgene 26969P (Lee et al., 2010)) targeted either left whisker primary sensory cortex (S1) or left whisker primary motor cortex (M1). Briefly, mice were anesthetized with isoflurane (4% induction, 0.8-1.5% maintenance) and placed onto a stereotaxic frame (Stoelting) that had a feedback controlled heating blanket maintained at 36℃ (FHC) on the base. The scalp was cleaned with Betadine (Purdue Products) followed by 70% ethanol (Fisher) three times.

Ketorolac (5 mg/kg) (Hospira) and Bupivacaine (0.25%) (0.1 mL, Fresenius Kabi) were injected subcutaneously into the left flank and scalp, respectively. A midline incision was made and the skull was exposed. The skull was leveled in the dorsoventral plane by ensuring equal bregma and lambda coordinates. For M1 and S1 injections, a craniotomy was made at the following coordinates (S1 coordinates with respect to bregma: AP = -1.0 mm; ML = +3.3 mm; DV = -0.6 mm; M1 coordinates with respect to bregma: anteroposterior (AP) = +1.6 mm; mediolateral (ML) = +1.5 mm; dorsoventral (DV) = -0.6 mm). In some mice, AAV5-Ef1a-DIO eNpHR 3.0-EYFP was injected into striatum (addgene 26966 (Saunders et al., 2012)) at the following coordinates (AP) = 1 mm; (ML) = 1.8 mm (DV) = -2.0 mm. The micropipette was slowly lowered to the proper depth and allowed to sit for 5 minutes. Following this, 210 nL of ChR2 virus solution or 280 nl of NpHR virus solution, diluted 1:1 with phosphate buffered saline was pressure injected over 5 minutes followed by a delay of an additional 5 minutes to allow for viral diffusion into the tissue. The micropipette was then slowly raised. The scalp was closed and secured with silk sutures and tissue glue. After surgery, mice were placed in clean, temporary housing and monitored for 72 hours. After this monitoring period, mice were transferred to their home cages and allowed to recover for at least 4 weeks before either electrophysiological or behavioral experiments, permitting viral expression in the M1 and S1 axon terminals located in the striatum.

***Ex vivo* whole cell current clamp recordings**

Mice were induced with isoflurane (3%) and deeply anesthetized with ketamine and xylazine (300/30 mg/kg, i.p.). Mice were then transcardially perfused with either cold or room temperature modified ACSF containing (in mM) NMDG 103, KCl 2.5, NaH_2PO_4 1.2, $NaHCO_3$ 30, HEPES 20, glucose 25, HCl 101, $MgSO_4$ 10 which was continuously bubbled with 95% O_2 5% CO_2. Coronal slices (300 µm) were cut on a Leica VT1200S vibratome. Following a short recovery in the same solution at 36°C, slices were transferred to ACSF which contained (in mM) NaCl 124, KCl 2.5, $NaHCO_3$ 26, NaH_2PO_4 1.2, glucose 10, pyruvate 3, $MgCl_2$ 1, and $CaCl_2$ 2 which was continuously bubbled with 95% O_2 and 5% CO_2 for at least one hour before recording. Recordings were obtained in the same solution. The pipette solution contained K methanesulfonate 130, KCl 10, HEPES 10, $MgCl_2$ 2, Na_2ATP 4, and Na_2GTP 0.4 at pH 7.25 and 290-295 mOsm/L. Patch pipettes (2-5 MΩ) were constructed from 2.0 mm o.d. borosilicate glass (Warner Instruments) pulled using a Sutter P-1000 horizontal puller. Current clamp recordings were obtained from identified neuron types using mice expressing tdTomato in D1-, D2-, or PV-expressing neurons. When recording from SPNs, unlabeled neurons were assumed to belong to the other projection neuron type when the neuron exhibited characteristic physiological properties of SPNs such as little to no sag in voltage response after hyperpolarizing current injection and a ramp depolarization and regular action potential firing in response to depolarizing current injection (Kawaguchi, 1993). Rarely, unlabeled neurons could be identified as a fast spiking interneuron based on physiological characteristics, the most prominent of which is a bursty action potential pattern in response to depolarizing current injection (Kawaguchi, 1993). Neurons were recorded in the dorsal striatum (approximately 1.4 to 0.5 mm anterior to bregma) which receives input from both S1 and M1 (Hooks et al., 2018; Hunnicutt et al., 2016; Ramanathan et al., 2002). Channelrhodopsin-2 (ChR2) was activated by illumination with a 2.5 ms, 460-500 nm LED light pulse (1.2 mW measured after the objective,

Thorlabs) delivered through the objective lens (40x) of an Olympus BX51WI microscope. Stimulation was presented once every 30 seconds for 20 sweeps. Slices were submerged and continuously superfused with ACSF during recording. Data were acquired with a HEKA EPC10 amplifier and digitized at 20 kHz in Patchmaster. Voltages reported in the example traces have not been corrected for the liquid junction potential.

Analysis of physiology data was carried out using custom scripts written in MATLAB. Single pulse postsynaptic potential amplitudes were calculated from averaged sweeps of up to 20 stimulations and were defined as the difference between the peak amplitude achieved within 500 ms centered around the time of optogenetic stimulation and the baseline membrane potential which itself was calculated as the average membrane potential between 1 s and 500 ms prior to optogenetic stimulation. Suprathreshold responses were excluded from analysis by removing sweeps containing action potentials from the average if only a small number of sweeps had action potentials in them or by estimating the size of the subthreshold PSP by filtering the data with a lowpass butterworth filter with a cutoff frequency of between 30 and 50 Hz. Traces were also excluded if the resting membrane potential drifted substantially as identified by visual inspection.

Train stimuli consisted of 2.5 ms pulses of light delivered at 25 Hz every 30 seconds for 5 sweeps. Sweeps were averaged and the amplitude of the PSPs calculated. Suprathreshold events were filtered with a lowpass butterworth filter with a cutoff frequency of 50 Hz. For each pulse interval, if the amplitude of the PSP was greater than 1.5 times the amplitude of the previous PSP, as would be the case in a suprathreshold response, filtered data was used to estimate the underlying PSP. If the first stimulation contained a suprathreshold response, filtered data was used for that pulse. The amplitude of the first PSP was calculated as 100% and amplitudes of subsequent PSPs in the train were calculated as a percentage of the first PSP.

Optical Cannula Implantation Surgery

Mice designated for behavior testing were allowed to recover for three weeks prior to the fiber optic implant surgery. Following the implant surgery, mice were allowed to recover for an additional week prior to handling. A custom head post was fitted to each mouse using methods similar to those previously described (Chen et al., 2013a, 2015; Lee and Margolis, 2016; Margolis et al., 2012). Briefly, mice were anesthetized with isoflurane (4% induction, 0.8-1.5% maintenance) and mounted onto a stereotaxic frame(Stoelting) with a feedback controlled heating blanket maintained at 36℃ (FHC) on the base. After the scalp was reflected, connective tissue was removed from the skull by gentle scraping and a blue light curable bonding agent (iBond, Heraeus Kulzer) was applied to the skull followed by a ring of dental composite around the outer edge (Charisma, Kulzer). A craniotomy was made above the left striatum for optical cannula insertion (coordinates with respect to bregma: AP = +1.0 mm; ML = +1.8 mm; DV = -2.0 mm). The optical cannula (length cut to 3 mm, 0.50 nA; 200 μm diameter; Thorlabs) was secured with dental composite (Tetric Evoflow, Ivoclar Vivadent). A custom aluminum head post (weight, < 1 g) was also cemented to the contralateral hemisphere. The scalp was closed around the resulting head cap using silk sutures and tissue glue.

After surgery, mice were allowed to recover in their home cages for one week before any handling was performed. Following the post-surgical recovery period, mice were handled daily for at least one week. During this handling period, mice were also acclimated to head fixation. This was done by placing them within a tube (length 14 cm; inner diameter 3.5 cm) attached to a custom platform (length 16.75 cm; width 12.25 cm). The platform contained an aluminum crossbar with screw holes to mount the head post and secure the mouse's head.

In Vivo Optogenetics

Two high-powered LEDs (ChR2; 460 nm; Halorhodopsin (NpHR); 520 nm; Prizmatix) and LED current drivers (Prizmatix) were used for *in vivo* optogenetics. M1-ChR2 mice were stimulated at low intensity (~3 mW), while S1-ChR2 and PV-ChR2 mice were stimulated at high intensity (~7.5 mW) for all behavioral tasks. Dual optogenetic mice (PV-NpHR and S1-ChR2) were stimulated at ~3.5 mW for the PV-NpHR and ~7.5 mW for the S1-ChR2. High intensity M1 stimulation was not used because it induced overt torso, limb, and facial movements, which interfered with licking. Stimulation of S1 at low intensities had no apparent effects on behavior. Stimulation intensity was kept consistent between mice in all three conditions by measuring the intensity prior to testing. A PMD-100D optical power meter (Thorlabs) was used to measure LED intensity.

Light was delivered to the cortical afferents and PV interneurons in the striatum through an optical fiber patchcord (Thorlabs; length 1 m; 0.50 nA; 200 μm diameter) connected to an optical cannula (described above) via a mating sleeve (Thorlabs). A small piece of heat shrink resistant tubing (Qualtek) was placed over the cannula during LED testing to prevent stray light during the task which might lead to texture illumination. A Pulse Pal (Sanders et al., 2014) activated the LED current driver with 5 ms pulses at 25 Hz for two seconds beginning when the texture was presented. Corticostriatal neurons are capable of following this 25 Hz firing rate (Oswald et al., 2013)

Go/No-Go Tactile Discrimination Task

Head-fixed mice were trained to utilize their whiskers to discriminate between two textures presented to the whiskers on a motorized stage in a random order based on custom-written code in LabVIEW (National Instruments). This software controlled a linear stage and stepper motor similar to previously described (Chen et al., 2013b; Lee and Margolis, 2016). The stepper motor rotated arms holding the two textures. Mice were trained to lick a piezo spout when presented with the "Go" texture (100 grit sandpaper; P100) and to withhold licking when presented with the "NoGo" texture (1200 grit sandpaper; P1200). A piezo film sensor that detected licks was connected to a solenoid-controlled water delivery spout. Additionally, a solenoid-controlled air spout was aimed at the contralateral mystacial pad. The texture task was carried out in a darkened room to minimize non-tactile cues. If mice correctly licked when presented with the Go texture, they were provided a small water reward (~5 μL). If mice incorrectly licked when presented with the NoGo texture, they were punished with a brief air puff. Sessions could be ended early if the mouse was no longer performing the task. Water was manually delivered ("autoreward") by the experimenter following 15 consecutive trials without

responding. If the mouse did not lick when water was present on the end of the spout following three autorewards, the session was ended.

Trials began with a 1 s pre-task interval, followed by texture movement toward the mice which was accompanied by a brief, cue tone (100 ms, 2930 Hz). Once the texture reached a set distance within reach of the whiskers, mice had a 2 s presentation time (PT) window to respond. A grace period was present during the initial 500 ms of the PT window where licks were not counted. Correctly licking in response to the Go texture (Hit) resulted in delivery of a water reward accompanied by a tone, while incorrectly licking in response to the NoGo texture (False Alarm; FA) resulted in a brief air puff (100-200 ms, 10-20 psi), a time-out period (7000-10000 ms), and an accompanying white noise. If no responding was detected to the Go or NoGo texture, the trial outcome was either a Miss or Correct Rejection (CR), respectively. During LED testing, a 2 s train of 5 ms pulses at 25 Hz accompanied the PT window. Once mice either responded or 2 seconds had elapsed, the texture retreated to a set distance followed by an inter-trial interval (ITI) of 2 s during which the next texture was rotated into position.

Behavioral training lasted up to 3 weeks and mice were tested twice daily. Training proceeded in three general steps, but sessions could be added to ensure that mice adequately learned each step. (1) An initial shaping session acclimated mice to licking for a water reward. Water is automatically provided at the end of the PT window even if the mouse doesn't lick. No texture is presented during this step. Each session consisted of 150 trials. (2) Only the Go texture is presented for two to three sessions, teaching mice to whisk against it and lick for a water reward. Each session consisted of 150 trials. (3) Both the Go and NoGo textures are presented at equal probabilities and no texture was presented for more than three consecutive trials. Mice were trained to whisk against the presented texture and respond appropriately. All sessions during the third step consisted of 127 trials. A subset of these sessions contained optogenetic stimulation. Sessions without optogenetic stimulation were interspersed to maintain behavioral performance. For single optogenetic stimulation testing (stimulation of S1 or M1 corticostriatal afferents or direct stimulation of PV-expressing interneurons), sessions were split into 50 baseline trials followed by 77 stimulation trials. For testing with dual optogenetic manipulation (stimulation of S1 corticostriatal afferents and inhibition of PV-expressing interneurons), sessions were divided into three blocks: 40 baseline trials, 40 S1-ChR2 stimulation trials and 47 S1-ChR2 and PV-NpHR stimulation trials. Stimulated and unstimulated data are from sessions where LED stimulation was administered. Certain sessions were excluded from analysis due to poor performance under control conditions such as excessive impulsivity as indicated by an increase in FA rate or decreased motivation to complete the task which was indicated by an increase in Misses. Behavioral performance was further monitored by computing each mouse's sensitivity (d') score after each session. This score is derived from signal detection theory (McNicol, 1970). A $d' < 1$ denoted non-expert performance, while a $d' > 1$ denoted expert performance. If a mouse's performance declined, it could be modulated by titrating water allowance or by training with more sessions without LED stimulation. At the end of behavioral testing, a single whisker trim control session was performed. The whiskers that were used to discriminate textures were unilaterally trimmed and performance was compared to the baseline period. Additionally, mice were tested while freely moving during open field (OF) and

rotarod (RR) assays to examine if generalized motor activity increased due to optical stimulation as described in the Supplemental Information.

Analysis and Statistics

Behavioral performance was measured using four indices: Hit Rate, FA Rate, Sensitivity, and Bias. Hit Rate was calculated by the following equation: [Hit/(Hit+Miss)], where Hit is the number of correct Go trials and Miss is the number of incorrect Go trials. A similar formula was used to calculate FA Rate: [FA/(FA+CR)], where FA is the number of incorrect NoGo trials and CR is the number of correct NoGo trials. Sensitivity was calculated with the following equation: [(normalized inverse(Hit Rate)-normalized inverse(FA Rate))]. Bias was calculated with the following equation: [0.5*(normalized inverse(Hit Rate)+normalized inverse(FA Rate))]. Sensitivity illustrates how well a mouse can discriminate between two textures by comparing the normalized Hit and FA Rates. Bias is a measure that is independent of sensitivity and it illustrates a mouse's overall responding, regardless of trial type.

Group data are presented as mean ± SEM. Statistics were calculated in MATLAB or SAS (SAS Institute). Data were analyzed and compared using paired *t*-tests, one-way Analysis of Variance (ANOVA), or Repeated Measures ANOVA followed by post-hoc Bonferroni multiple comparison tests or paired contrasts respectively. In all cases, effects were considered significant at $p < 0.05$.

References:

Ade, K.K., Wan, Y., Chen, M., Gloss, B., and Calakos, N. (2011). An Improved BAC Transgenic Fluorescent Reporter Line for Sensitive and Specific Identification of Striatonigral Medium Spiny Neurons. Front. Syst. Neurosci. *5,* 32.

Albin, R.L., Young, A.B., and Penney, J.B. (1989). The functional anatomy of basal ganglia disorders. Trends Neurosci. *12,* 366–375.

Alloway, K.D., Smith, J.B., Mowery, T.M., and Watson, G.D.R. (2017). Sensory Processing in the Dorsolateral Striatum: The Contribution of Thalamostriatal Pathways. Front. Syst. Neurosci. *11,* 53.

Aronoff, R., Matyas, F., Mateo, C., Ciron, C., Schneider, B., and Petersen, C.C.H. (2010). Long-range connectivity of mouse primary somatosensory barrel cortex. Eur. J. Neurosci. *31,* 2221–2233.

Assous, M., and Tepper, J.M. (2018). Excitatory extrinsic afferents to striatal interneurons and interactions with striatal microcircuitry. Eur. J. Neurosci.

Assous, M., Kaminer, J., Shah, F., Garg, A., Koós, T., and Tepper, J.M. (2017). Differential processing of thalamic information via distinct striatal interneuron circuits. Nat. Commun. *8,* 15860.

Bennett, B.D., and Bolam, J.P. (1994). Synaptic input and output of

parvalbumin-immunoreactive neurons in the neostriatum of the rat. Neuroscience *62,* 707–719.

Bosman, L.W.J., Houweling, A.R., Owens, C.B., Tanke, N., Shevchouk, O.T., Rahmati, N., Teunissen, W.H.T., Ju, C., Gong, W., Koekkoek, S.K.E., et al. (2011). Anatomical pathways involved in generating and sensing rhythmic whisker movements. Front. Integr. Neurosci. *5,* 53.

Burguière, E., Monteiro, P., Feng, G., and Graybiel, A.M. (2013). Optogenetic stimulation of lateral orbitofronto-striatal pathway suppresses compulsive behaviors. Sci. *340,* 1243–1246.

Chen, J.L., Carta, S., Soldado-Magraner, J., Schneider, B.L., and Helmchen, F. (2013a). Behaviour-dependent recruitment of long-range projection neurons in somatosensory cortex. Nature *499,* 336–340.

Chen, J.L., Pfäffli, O.A., Voigt, F.F., Margolis, D.J., and Helmchen, F. (2013b). Online correction of licking-induced brain motion during two-photon imaging with a tunable lens. J. Physiol. *591,* 4689–4698.

Chen, J.L., Margolis, D.J., Stankov, A., Sumanovski, L.T., Schneider, B.L., and Helmchen, F. (2015). Pathway-specific reorganization of projection neurons in somatosensory cortex during learning. Nat. Neurosci. *18,* 1101–1108.

Crochet, S., Lee, S.-H., and Petersen, C.C.H. (2018). Neural Circuits for Goal-Directed Sensorimotor Transformations. Trends Neurosci.

DeLong, M.R. (1990). Primate models of movement disorders of basal ganglia origin. Trends Neurosci. *13,* 281–285.

Diamond, M.E., von Heimendahl, M., Knutsen, P.M., Kleinfeld, D., and Ahissar, E. (2008). “Where” and “what” in the whisker sensorimotor system. Nat. Rev. Neurosci. *9,* 601–612.

Díaz-Hernández, E., Contreras-López, R., Sánchez-Fuentes, A., Rodríguez-Sibrían, L., Ramírez-Jarquín, J.O., and Tecuapetla, F. (2018). The Thalamostriatal Projections Contribute to the Initiation and Execution of a Sequence of Movements. Neuron.

Ebbesen, C.L., Doron, G., Lenschow, C., and Brecht, M. (2017). Vibrissa motor cortex activity suppresses contralateral whisking behavior. Nat. Neurosci. *20,* 82–89.

Feldmeyer, D., Brecht, M., Helmchen, F., Petersen, C.C.H., Poulet, J.F.A., Staiger, J.F., Luhmann, H.J., and Schwarz, C. (2013). Barrel cortex function. Prog. Neurobiol. *103,* 3–27.

Ferezou, I., Haiss, F., Gentet, L.J., Aronoff, R., Weber, B., and Petersen, C.C.H. (2007). Spatiotemporal dynamics of cortical sensorimotor integration in behaving mice. Neuron *56,* 907–923.

Gerfen, C.R., Engber, T.M., Mahan, L.C., Susel, Z., Chase, T.N., Monsma, F.J., and Sibley, D.R. (1990). D1 and D2 dopamine receptor-regulated gene expression of striatonigral and striatopallidal neurons. Sci. *250,* 1429–1432.

Gerfen, C.R., Paletzki, R., and Heintz, N. (2013). GENSAT BAC cre-recombinase driver lines to study the functional organization of cerebral cortical and basal ganglia circuits. Neuron *80,* 1368–1383.

Gittis, A.H., Nelson, A.B., Thwin, M.T., Palop, J.J., and Kreitzer, A.C. (2010). Distinct roles of GABAergic interneurons in the regulation of striatal output pathways. J. Neurosci. Off. J. Soc. Neurosci. *30,* 2223–2234.

Gittis, A.H., Leventhal, D.K., Fensterheim, B.A., Pettibone, J.R., Berke, J.D., and Kreitzer, A.C. (2011). Selective inhibition of striatal fast-spiking interneurons causes dyskinesias. J. Neurosci. : Off. J. Soc. Neurosci. *31,* 15727–15731.

Guo, Q., Wang, D., He, X., Feng, Q., Lin, R., Xu, F., Fu, L., and Luo, M. (2015). Whole-brain mapping of inputs to projection neurons and cholinergic interneurons in the dorsal striatum. PloS One *10,* e0123381.

Guo, Z.V., Li, N., Huber, D., Ophir, E., Gutnisky, D., Ting, J.T., Feng, G., and Svoboda, K. (2014a). Flow of cortical activity underlying a tactile decision in mice. Neuron *81,* 179–194.

Guo, Z.V., Hires, S.A., Li, N., O'Connor, D.H., Komiyama, T., Ophir, E., Huber, D., Bonardi, C., Morandell, K., Gutnisky, D., et al. (2014b). Procedures for behavioral experiments in head-fixed mice. PloS One *9,* e88678.

Helmchen, F., Gilad, A., and Chen, J.L. (2018). Neocortical dynamics during whisker-based sensory discrimination in head-restrained mice. Neuroscience *368,* 57–69.

Hippenmeyer, S., Vrieseling, E., Sigrist, M., Portmann, T., Laengle, C., Ladle, D.R., and Arber, S. (2005). A developmental switch in the response of DRG neurons to ETS transcription factor signaling. PLoS Biol. *3,* e159.

Hooks, B.M., Papale, A.E., Paletzki, R.F., Feroze, M.W., Eastwood, B.S., Couey, J.J., Winnubst, J., Chandrashekar, J., and Gerfen, C.R. (2018). Topographic precision in sensory and motor corticostriatal projections varies across cell type and cortical area. Nat. Commun. *9,* 3549.

Hunnicutt, B.J., Jongbloets, B.C., Birdsong, W.T., Gertz, K.J., Zhong, H., and Mao, T. (2016). A comprehensive excitatory input map of the striatum reveals novel functional organization. ELife *5.*

Jahfari, S., Waldorp, L., van den Wildenberg, W.P.M., Scholte, H.S., Ridderinkhof, K.R., and Forstmann, B.U. (2011). Effective connectivity reveals important roles for both the hyperdirect (fronto-subthalamic) and the indirect (fronto-striatal-pallidal) fronto-basal ganglia pathways during response inhibition. J. Neurosci. Off. J. Soc. Neurosci. *31,* 6891–6899.

Kawaguchi, Y. (1993). Physiological, morphological, and histochemical characterization of three classes of interneurons in rat neostriatum. J. Neurosci. Off. J. Soc. Neurosci. *13,* 4908–4923.

Kim, C.K., Adhikari, A., and Deisseroth, K. (2017). Integration of optogenetics with complementary methodologies in systems neuroscience. Nat. Rev. Neurosci. *18,* 222–235.

Klug, J.R., Engelhardt, M.D., Cadman, C.N., Li, H., Smith, J.B., Ayala, S., Williams, E.W., Hoffman, H., and Jin, X. (2018). Differential inputs to striatal cholinergic and parvalbumin interneurons imply functional distinctions. ELife *7.*

Koós, T., and Tepper, J.M. (1999). Inhibitory control of neostriatal projection neurons by

GABAergic interneurons. Nat. Neurosci. *2,* 467–472.

Kravitz, A.V., Freeze, B.S., Parker, P.R.L., Kay, K., Thwin, M.T., Deisseroth, K., and Kreitzer, A.C. (2010). Regulation of parkinsonian motor behaviours by optogenetic control of basal ganglia circuitry. Nature *466,* 622–626.

Kress, G.J., Yamawaki, N., Wokosin, D.L., Wickersham, I.R., Shepherd, G.M.G., and Surmeier, D.J. (2013). Convergent cortical innervation of striatal projection neurons. Nat. Neurosci. *16,* 665–667.

Kwon, S.E., Yang, H., Minamisawa, G., and O'Connor, D.H. (2016). Sensory and decision-related activity propagate in a cortical feedback loop during touch perception. Nat. Neurosci. *19,* 1243–1249.

Lee, C.R., and Margolis, D.J. (2016). Pupil Dynamics Reflect Behavioral Choice and Learning in a Go/NoGo Tactile Decision-Making Task in Mice. Front. Behav. Neurosci. *10,* 200.

Lee, J.H., Durand, R., Gradinaru, V., Zhang, F., Goshen, I., Kim, D.-S., Fenno, L.E., Ramakrishnan, C., and Deisseroth, K. (2010). Global and local fMRI signals driven by neurons defined optogenetically by type and wiring. Nature *465,* 788–792.

Lee, K., Holley, S.M., Shobe, J.L., Chong, N.C., Cepeda, C., Levine, M.S., and Masmanidis, S.C. (2017). Parvalbumin Interneurons Modulate Striatal Output and Enhance Performance during Associative Learning. Neuron *93,* 1451–1463.e4.

Leinweber, M., Ward, D.R., Sobczak, J.M., Attinger, A., and Keller, G.B. (2017). A Sensorimotor Circuit in Mouse Cortex for Visual Flow Predictions. Neuron *95,* 1420–1432.e5.

Madisen, L., Zwingman, T.A., Sunkin, S.M., Oh, S.W., Zariwala, H.A., Gu, H., Ng, L.L., Palmiter, R.D., Hawrylycz, M.J., Jones, A.R., et al. (2010). A robust and high-throughput Cre reporting and characterization system for the whole mouse brain. Nat. Neurosci. *13,* 133–140.

Madisen, L., Mao, T., Koch, H., Zhuo, J., Berenyi, A., Fujisawa, S., Hsu, Y.-W.A., Garcia, A.J., Gu, X., Zanella, S., et al. (2012). A toolbox of Cre-dependent optogenetic transgenic mice for light-induced activation and silencing. Nat. Neurosci. *15,* 793–802.

Mallet, N., Le Moine, C., Charpier, S., and Gonon, F. (2005). Feedforward inhibition of projection neurons by fast-spiking GABA interneurons in the rat striatum in vivo. J. Neurosci. Off. J. Soc. Neurosci. *25,* 3857–3869.

Mao, T., Kusefoglu, D., Hooks, B.M., Huber, D., Petreanu, L., and Svoboda, K. (2011). Long-range neuronal circuits underlying the interaction between sensory and motor cortex. Neuron *72,* 111–123.

Margolis, D.J., Lütcke, H., Schulz, K., Haiss, F., Weber, B., Kügler, S., Hasan, M.T., and Helmchen, F. (2012). Reorganization of cortical population activity imaged throughout long-term sensory deprivation. Nat. Neurosci. *15,* 1539–1546.

Matyas, F., Sreenivasan, V., Marbach, F., Wacongne, C., Barsy, B., Mateo, C., Aronoff, R., and Petersen, C.C.H. (2010). Motor control by sensory cortex. Sci. *330,* 1240–1243.

McNicol, D. (1970). A primer of signal detection theory (Allen and Unwin).

Melzer, S., Gil, M., Koser, D.E., Michael, M., Huang, K.W., and Monyer, H. (2017). Distinct Corticostriatal GABAergic Neurons Modulate Striatal Output Neurons and Motor Activity. Cell Reports *19,* 1045–1055.

Mink, J.W. (1996). The basal ganglia: focused selection and inhibition of competing motor programs. Prog. Neurobiol. *50,* 381–425.

Mink, J.W. (2003). The Basal Ganglia and involuntary movements: impaired inhibition of competing motor patterns. Arch. Neurol. *60,* 1365–1368.

Muñoz-Manchado, A.B., Bengtsson Gonzales, C., Zeisel, A., Munguba, H., Bekkouche, B., Skene, N.G., Lönnerberg, P., Ryge, J., Harris, K.D., Linnarsson, S., et al. (2018). Diversity of Interneurons in the Dorsal Striatum Revealed by Single-Cell RNA Sequencing and PatchSeq. Cell Reports *24,* 2179–2190.e7.

Ni, J., and Chen, J.L. (2017). Long-range cortical dynamics: a perspective from the mouse sensorimotor whisker system. Eur. J. Neurosci. *46,* 2315–2324.

Obeso, I., Wilkinson, L., Casabona, E., Speekenbrink, M., Luisa Bringas, M., Álvarez, M., Álvarez, L., Pavón, N., Rodríguez-Oroz, M.C., Macías, R., et al. (2014). The subthalamic nucleus and inhibitory control: impact of subthalamotomy in Parkinson's disease. Brain: J. Neurol. *137,* 1470–1480.

O'Connor, D.H., Huber, D., and Svoboda, K. (2009). Reverse engineering the mouse brain. Nature *461,* 923–929.

O'Hare, J.K., Li, H., Kim, N., Gaidis, E., Ade, K., Beck, J., Yin, H., and Calakos, N. (2017). Striatal fast-spiking interneurons selectively modulate circuit output and are required for habitual behavior. ELife *6.*

Oswald, M.J., Tantirigama, M.L.S., Sonntag, I., Hughes, S.M., and Empson, R.M. (2013). Diversity of layer 5 projection neurons in the mouse motor cortex. Front. Cell. Neurosci. *7,* 174.

Parthasarathy, H.B., and Graybiel, A.M. (1997). Cortically driven immediate-early gene expression reflects modular influence of sensorimotor cortex on identified striatal neurons in the squirrel monkey. J. Neurosci. Off. J. Soc. Neurosci. *17,* 2477–2491.

Petersen, C.C.H. (2014). Cortical control of whisker movement. Annu. Rev. Neurosci. *37,* 183–203.

Ramanathan, S., Hanley, J.J., Deniau, J.-M., and Bolam, J.P. (2002). Synaptic convergence of motor and somatosensory cortical afferents onto GABAergic interneurons in the rat striatum. J. Neurosci. : Off. J. Soc. Neurosci. *22,* 8158–8169.

Reig, R., and Silberberg, G. (2014). Multisensory integration in the mouse striatum. Neuron *83,* 1200–1212.

Reig, R., and Silberberg, G. (2016). Distinct Corticostriatal and Intracortical Pathways Mediate Bilateral Sensory Responses in the Striatum. Cereb. Cortex *26,* 4405–4415.

Roseberry, T., and Kreitzer, A. (2017). Neural circuitry for behavioural arrest. Philos. Trans. R. Soc. London. Ser. B, Biol. Sci. *372.*

Saunders, A., Johnson, C.A., and Sabatini, B.L. (2012). Novel recombinant adeno-associated viruses for Cre activated and inactivated transgene expression in neurons. Front. Neural Circuits *6,* 47.

Schmidt, R., Leventhal, D.K., Mallet, N., Chen, F., and Berke, J.D. (2013). Canceling actions involves a race between basal ganglia pathways. Nat. Neurosci. *16,* 1118–1124.

Schneider, D.M., Nelson, A., and Mooney, R. (2014). A synaptic and circuit basis for corollary discharge in the auditory cortex. Nature *513,* 189–194.

Sciamanna, G., Ponterio, G., Mandolesi, G., Bonsi, P., and Pisani, A. (2015). Optogenetic stimulation reveals distinct modulatory properties of thalamostriatal vs corticostriatal glutamatergic inputs to fast-spiking interneurons. Sci. Reports *5,* 16742.

Sippy, T., Lapray, D., Crochet, S., and Petersen, C.C.H. (2015). Cell-Type-Specific Sensorimotor Processing in Striatal Projection Neurons during Goal-Directed Behavior. Neuron *88,* 298–305.

Sreenivasan, V., Esmaeili, V., Kiritani, T., Galan, K., Crochet, S., and Petersen, C.C.H. (2016). Movement Initiation Signals in Mouse Whisker Motor Cortex. Neuron *92,* 1368–1382.

Tecuapetla, F., Jin, X., Lima, S.Q., and Costa, R.M. (2016). Complementary Contributions of Striatal Projection Pathways to Action Initiation and Execution. Cell *166,* 703–715.

Tepper, J.M., Tecuapetla, F., Koós, T., and Ibáñez-Sandoval, O. (2010). Heterogeneity and diversity of striatal GABAergic interneurons. Front. Neuroanat. *4,* 150.

Xiong, Q., Znamenskiy, P., and Zador, A.M. (2015). Selective corticostriatal plasticity during acquisition of an auditory discrimination task. Nature *521,* 348–351.

Xu, N., Harnett, M.T., Williams, S.R., Huber, D., O'Connor, D.H., Svoboda, K., and Magee, J.C. (2012). Nonlinear dendritic integration of sensory and motor input during an active sensing task. Nature *492,* 247–251.

Yamashita, T., and Petersen, C.C. (2016). Target-specific membrane potential dynamics of neocortical projection neurons during goal-directed behavior. ELife *5.*

Yamashita, T., Pala, A., Pedrido, L., Kremer, Y., Welker, E., and Petersen, C.C.H. (2013). Membrane potential dynamics of neocortical projection neurons driving target-specific signals. Neuron *80,* 1477–1490.

Supplemental Information

Supplemental Methods

Open Field Locomotor Behavior

Open field locomotor behavior was assessed by allowing mice to freely explore a 42 cm x 22 cm x 20 cm (LxWxH) polycarbonate laboratory arena (a rat cage with no bedding). It was placed inside a dark behavioral testing room. The cage was evenly illuminated using both red (Prophotonix) and infrared (Advanced Illumination) spotlights for automated mouse tracking. The optical fiber patchcord (Thorlabs) was connected to the mouse prior to being placed in the arena. LED stimulation with 5 ms pulses at 25 Hz occurred continuously during each 2 minute stimulation period. A video camera (Manta GigE, Allied Vision) mounted above the arena and Streampix 6 software (NorPix) were used to record the animal's movements at a frame rate of 25 Hz with frame triggering controlled by a Pulse Pal (Open Ephys). The arena was cleaned with 70% ethanol between mice to eliminate sensory cues that might influence exploration and sanitized with 10% bleach each day.

Testing took two days to complete with a single session per day. On day one, mice were allowed to freely explore the arena for 30 minutes with the patchcord attached to the cannula. On day two, mice were habituated inside the arena for 10 minutes. Following the habituation period, the mice followed a block trial order consisting of 3 conditions (No Stim exploration, exploration during optogenetic stimulation, and freely moving intertrial interval) that lasted 2 minutes each. This block design was repeated three times. Videos were recorded and saved for each No Stim and Stim period. These videos were analyzed offline using a custom-written MATLAB (Mathworks) algorithm that segmented the mouse profile and calculated a centroid value (in pixels) for each frame and distance traveled was calculated. Counterbalancing was not needed as each Stim period was followed by a Freely Moving period that prevented carryover effects of stimulation. Both habituation periods minimized anxiety or exploratory effects.

Accelerating Rotarod Test

A rotarod (ENV-576M, Med Associates) was set to accelerate from 4 to 40 rpm over 5 minutes and. Trials ended when mice fell off the rod or after 5 minutes had elapsed. If a mouse stopped ambulating and instead clutched the rotarod, the trial was considered ended when the mouse made a complete revolution around the rod. Data were recorded as latency to fall or end of the trial. The entire apparatus was cleaned with 70% ethanol between mice and sanitized with 10% bleach following all sessions.

Testing took two days to complete with a single session per day. On day one, mice were habituated at a fixed speed of 4 rpm for 2 minutes followed by a 7 minute ITI. This was done 3 times for each mouse. On day two, stimulation was introduced using the parameters described above throughout the entire 5 minute trial unless the trial was ended by the mouse falling or clutching the rod. The first two trials were No Stim trials with the first trial not being used in the final analysis to allow the mouse to practice the task. After the first two No Stim trials, the next trial was a Stim trial that was followed by a No Stim trial. This order was repeated (No Stim, Stim, No Stim, Stim, No Stim) until two stimulation trials had been performed and the test ended

on a No Stim trial. After each trial, mouse had a 7 minute ITI. Trials were counterbalanced when appropriate to ensure there were no carryover effects.

Histology

Following all testing, mice were deeply anesthetized with Ketamine-Xylazine (300 mg/kg Ketamine; 30 mg/kg Xylazine; i.p.) and transcardially perfused with PBS followed by 4% paraformaldehyde. The brain was carefully extracted and stored for 24 hours in 4% paraformaldehyde at 4℃. After, the brain was stored in 30% sucrose in PBS Azide at 4℃ until the brain had sunk. The tissue was sectioned at 40 µm with a Thermo Fisher Scientific Shandon Cryotome FSE cryostat in the coronal plane. Sections were mounted on slides and coverslipped with Aqua-Mount (Thermo Scientific). Fluorescent photomicrographs were obtained using a Zeiss AxioObserver Z1 inverted fluorescence microscope. Verification of injection site, cannula placement, and viral expression were obtained using the mosaic tile function of the Zeiss software at 5x, 20x, and 40x objectives.

Supplemental Results

Viral injections caused dense expression of ChR2

Injection of (AAV1.CaMKIIa.HChR2(H134R) -eYFP.WPRE.hGH) into either S1 or M1 resulted in dense expression in cortex demonstrating successful transfection and expression of ChR2 (**Figure S1**).

ANOVA comparing baseline of M1, S1, PV, and dual opto mice

One-way ANOVAs were used to determine whether significant differences existed between the baseline behavior of M1, S1, PV, and dual opto mice in the tactile Go/NoGo task. None of our four parameters exhibited significantly different baselines between our four groups (Lowest p-value (Sensitivity): ($F_{(3, 18)} = 1.42$, $p = 0.269$); Highest p-value (Hit Rate): ($F_{(3, 18)} = 0.662$, $p = 0.625$)).

Changes in responding are not generalized changes in motor behavior

To investigate whether the optogenetic stimulations used resulted in overall changes in motor behavior, we utilized open field and rotarod tests to assess the effects of stimulation on movement. For the open field test, there were no significant differences in total distance between the baseline and stimulation period for all three groups (M1: $p = 0.498$, $n = 6$; S1: $p = 0.505$, $n = 5$; PV: $p = 0.101$, $n = 6$; **Figure S2**). For the rotarod test, there were no significant differences in latency to fall between the baseline and stimulation periods for all three groups (M1: $p = 0.105$, $n = 5$; S1: $p = 0.087$, $n = 5$; PV: $p = 0.573$, $n = 6$; **Figure S2**). Additionally, the weight, ranging from 21.0g to 30.0g, showed no correlation with the latency to fall using linear regression ($r^2 = 0.0113$, $n = 18$). One-way ANOVAs were used to determine whether significant differences existed between the baselines of each group. Neither the open field or rotarod baselines were significantly different between the three groups (OF: ($F_{(2, 14)} = 0.277$, $p = 0.762$); RR: ($F_{(2, 13)} = 3.186$, $p = 0.075$)). Thus, the changes in tactile discrimination behavior observed during LED stimulation are task-specific and not generalized motor changes.

Mice used their whiskers to perform the task

We assessed if the mice primarily used their whiskers to perform the texture discrimination task. After 50 baseline trials were performed, the whiskers were trimmed unilaterally and an additional 100 trials were performed. Each parameter assessed during the texture discrimination task (Hit Rate, FA Rate, Sensitivity, and Bias) decreased significantly after the whiskers were trimmed ($n = 12$). Hit Rate (0.78 ± 0.05 to 0.23 ± 0.08; $p = 0.00002$), FA Rate (0.27 ± 0.05 to 0.12 ± 0.03 ;$p = 0.01$), Sensitivity (1.72 ± 0.32 to 0.28 ± 0.28; $p = 0.002$), and Bias (0.03 ± 0.16 to -1.33 ± 0.27; $p = 0.0003$) decreased significantly (**Figure S3**). Thus, the whiskers are necessary for discrimination task performance, indicating the mice do not rely on other off-target sensory modalities during task performance.

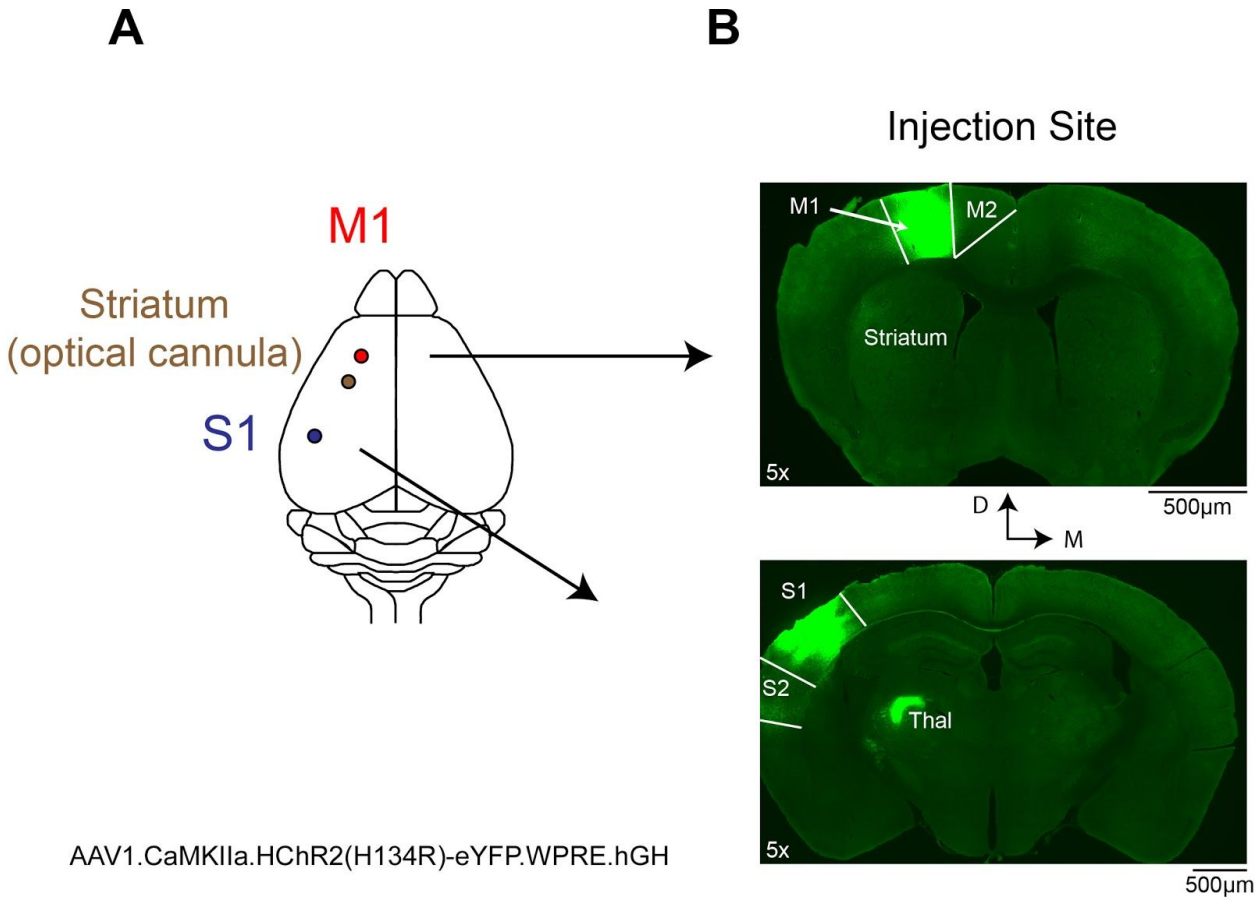

Figure S1: Expression of ChR2 in anatomically identified regions of cortex. **(A)** Schematic illustrating locations of viral (AAV1.CaMKIIa.HChR2(H134R)-eYFP.WPRE.hGH) injections into M1 (orange) and S1 (red) and optical cannula placement in the striatum. **(B)** *Top:* Coronal section through frontal cortex (X5), showing expression in primary motor (M1) cortical areas. *Bottom:* Coronal section through a more posterior section (X5), showing expression in primary sensory barrel cortex (S1 BC). Thal (thalamus).

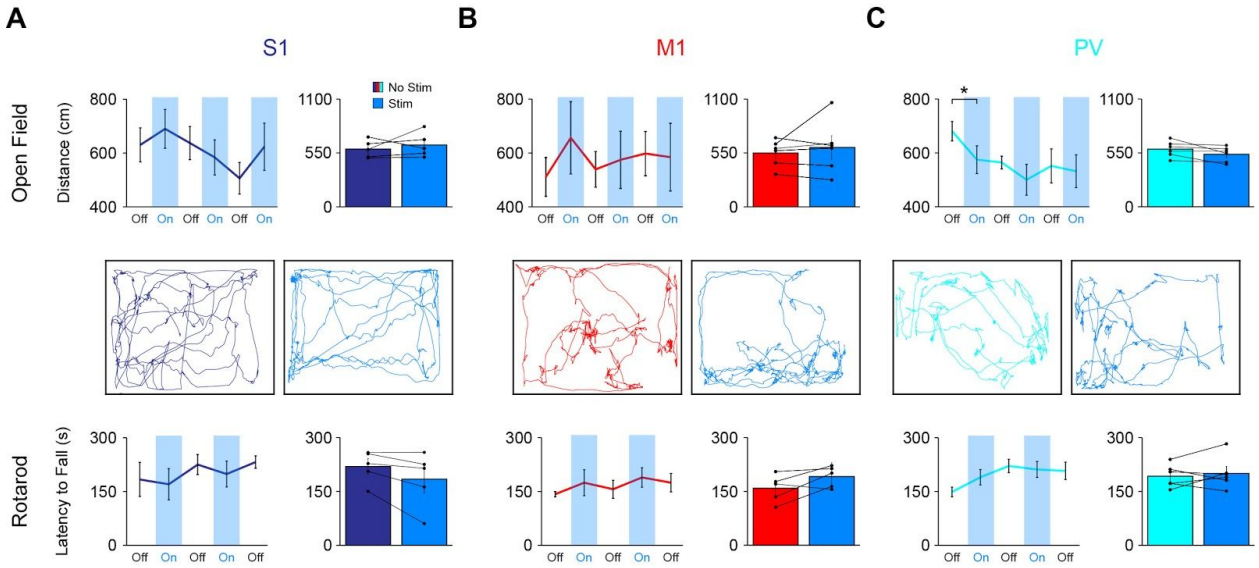

Figure S2: Stimulation of S1 or M1 corticostriatal afferents or PV striatal interneurons does not affect general motor behavior. **(A)** *Top left* Average total distance (± SEM) walked during 2 minute periods when S1 terminals (n = 5), **(B)** M1 terminals (n = 6), or **(C)** PV interneurons (n = 6) in the striatum were stimulated (blue) compared to not stimulated (white) in an open field task. *Top Right:* Mean of total distance traveled (± SEM) for **(A)** S1 terminals (n = 5), **(B)** M1 terminals (n = 6), or **(C)** PV interneurons (n = 6) in the striatum during baseline and stimulation periods. *Middle:* Representative tracking during 2 minute (*Left*) baseline and (*Right*) stimulation period in OF arena for **(A)** S1, **(B)** M1, and **(C)** PV conditions. *Bottom Left:* Average latency to fall (± SEM) when **(A)** S1 terminals (n = 5), **(B)** M1 terminals (n = 5), or **(C)** PV interneurons (n = 6) were either not stimulated (white) or stimulated (blue) on a rotarod task. Stimulation protocol was the same as the behavioral task and lasted up to 5 minutes. A 7 minute ITI followed each trial, allowing ample time for mice to recover, as well as precluding any lingering LED effects. *Bottom Right:* Grand mean (± SEM) for **(A)** S1 terminals (n = 5), **(B)** M1 terminals (n = 5), or **(C)** PV interneurons during baseline and stimulation periods. Student's t-tests were performed. *$p < 0.05$.

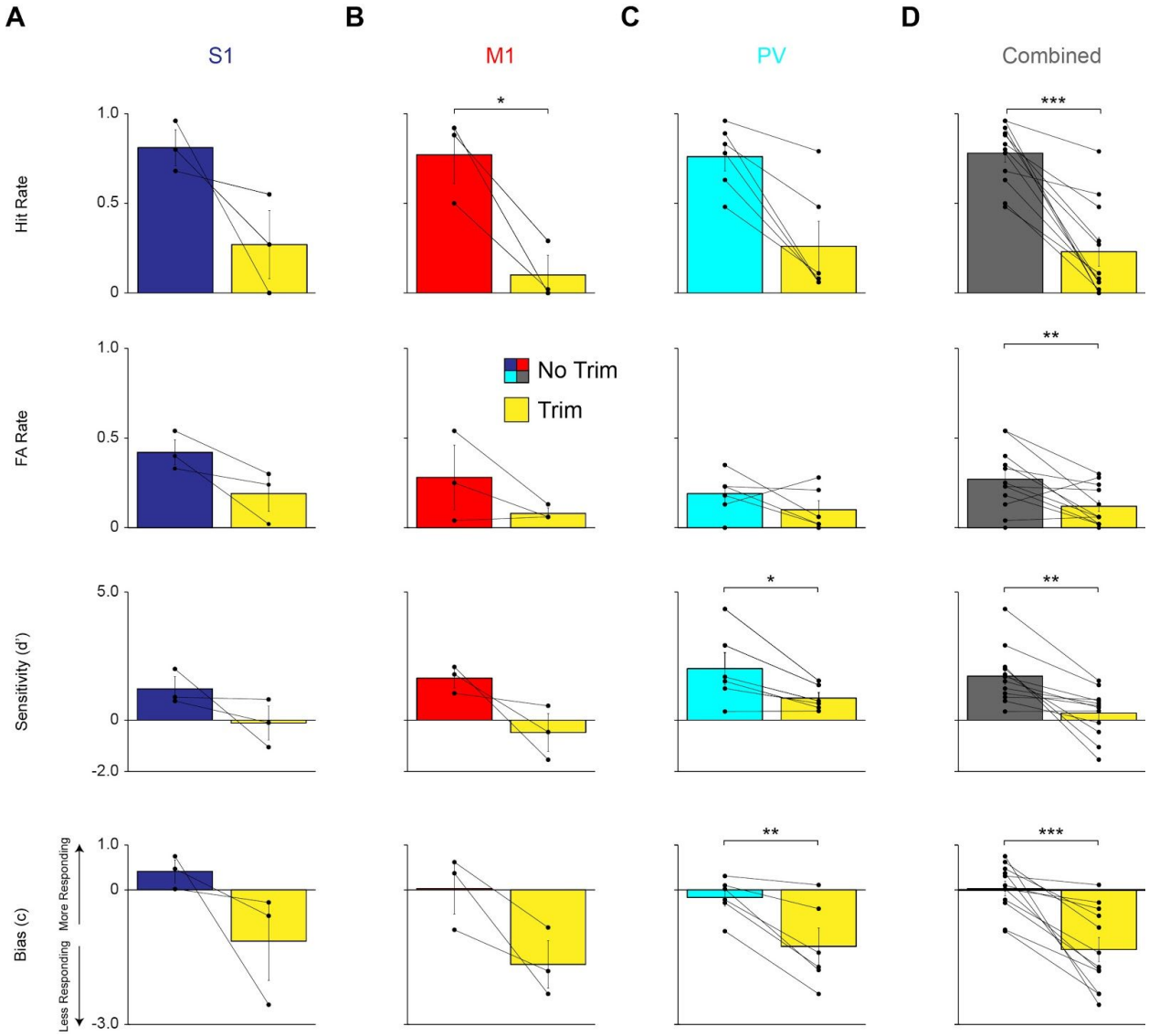

Figure S3: The texture discrimination task is dependent on tactile input. Whiskers used during the sensorimotor choice task were unilaterally trimmed following 50 pre-trim trials. 100 post-trim trials were run and behavioral performance, based on our four parameters, was compared. Grand mean (± SEM) for pre- and post-whisker trim for **(A)** S1 (n = 3), **(B)** M1 (n = 3), **(C)** PV (n = 6), and **(D)** Combined (n = 12) conditions are shown based on each of the four parameters. *$p < 0.05$, **$p < 0.01$, ***$p < 0.001$.